

X-Ray Absorption from the Milky Way Halo and the Local Group

Joel N. Bregman and Edward J. Lloyd-Davies

University of Michigan, Department of Astronomy, Ann Arbor, MI 48109

`jbregman@umich.edu, ejdavies@umich.edu`

ABSTRACT

Million degree gas is present at near-zero redshift and is due either to a gaseous Galactic Halo or a more diffuse but very massive Local Group medium. We can discriminate between these models because the column densities should depend on location in the sky, either relative to the Galaxy bulge or to the M31-Milky Way axis. To search for these signatures, we measured the O VII $K\alpha$ absorption line strength toward 25 bright AGNs, plus LMC X-3, using *XMM-Newton RGS* archival data. The data are in conflict with a purely Local Group model, but support the Galactic Halo model. The strongest correlation is between the O VII equivalent widths and the *ROSAT* background emission measurement in the R45 band (0.4-1 keV), for which O VII emission makes the largest single contribution. This suggests that much of the O VII emission and absorption are cospatial, from which the radius of a uniform halo appears to lie the range 15-110 kpc. The present data do not constrain the type of halo gas model and an equally good fit is obtained in a model where the gas density decreases as a power-law, such as $r^{-3/2}$. For a uniform halo with a radius of 20 kpc, the electron density would be $9 \times 10^{-4} \text{ cm}^{-3}$, and the gas mass is $4 \times 10^8 M_{\odot}$. The redshift of the four highest S/N O VII measurements is consistent with a Milky Way origin rather than a Local Group origin.

Subject headings: Galaxy: halo — ISM: abundances — Local Group — X-rays: diffuse background

1. Introduction

One of the important recent results from *Chandra*, *XMM*, and *FUSE* is the detection of hot gas at nearly zero redshift. The low redshift of the gas implies that it is either in the Local Group or in a halo around the Milky Way, and discriminating between these two possibilities is critical. If the gas is extended and fills the Local Group on the Mpc scale,

its mass exceeds the baryonic mass in all other galaxies in the Local Group. This would account for some of the “missing baryons” in the Local Universe, of fundamental importance for cosmology. Alternatively, if the gas is local to the Milky Way, within a 100 kpc region, the baryonic mass is two orders of magnitude lower and it would not dominate the local baryon content.

The tracers for this hot gaseous medium are the lines from common ions that occur in the $10^6 - 10^7$ K range, most notably O VII and O VIII. These X-ray lines have been observed in absorption (Nicastro et al. 2002; Rasmussen et al. 2003) with both *Chandra* and *XMM*, and in emission with a quantum-microcalorimeter spectrograph on a *Shuttle* payload, DXS (McCammon et al. 2002). In addition, the O VI ion, most common in $10^{5.5}$ K gas, has been studied in over 100 sightlines with *FUSE* (Sembach et al. 2003; Wakker et al. 2003).

The location and mass of the hot gas depends strongly on the assumed relationships between the ions. If O VI, O VII, and O VIII are cospatial, Nicastro et al. (2002) cannot find a pure collisional model at a single temperature. However, he can fit his data with a low density medium where photoionization is important, with a temperature of 2.5×10^5 K, a gas density of $n_e \approx 6 \times 10^{-6} \text{ cm}^{-3}$, and a pathlength of 3 Mpc, corresponding to a gas mass of $1.7 \times 10^{13} M_\odot$. This gas mass is considerably greater than the mass of all stars and cold gas within this volume, which is about $2 \times 10^{11} M_\odot$ and $1.2 \times 10^{10} M_\odot$, respectively (Braun 1991; Cox 2000; van den Bergh 2000; Carignan et al. 2006). This “Local Group Model” would help explain the missing baryons in the local universe.

Alternatively, Rasmussen et al. (2003) assume that only the X-ray lines are cospatial, primarily O VII and O VIII, leaving out O VI. They fix the temperature from the O VIII/O VII ratio, and, including the emission observations, find that a collisional ionization model is possible with a length scale of 0.15-1 Mpc. Their result implies a Local Group medium with masses of $10^{13} M_\odot$ for the 1 Mpc length scale, and $10^{11} M_\odot$ for the 0.15 Mpc length scale, still more gas than the collective ISM of Local Group galaxies. Recently, Fang et al. (2006) pointed out the sensitivity of this result to temperature and for a somewhat lower permitted temperature, smaller length scales are allowed, typical of a Galactic halo (50 kpc), and leading to considerably reduced gas masses.

In yet another approach, one might assume that the O VII emission and absorption are from the same gas, with some of the O VIII and O VI originating in other material. The X-ray emission line data was obtained with the inaugural flight of a quantum calorimeter rocket flight by McCammon et al. (2002) where they detected individual spectral lines responsible for much of the soft X-ray background, leading to an emission measure and metallicity. With an emission measure (n^2L) and an absorption column (nL), the size of the region L can be obtained and this leads to $L \approx 50$ kpc (Sanders et al. 2002), although this is a lower limit if

one allows for filling factors below unity. For filling factors near unity, this solution describes a halo around the Galaxy where the gas density is $n_e \sim 10^{-4} \text{ cm}^{-3}$ and the hot gas mass is $\sim 10^9\text{-}10^{10} M_\odot$, 2-3 orders of magnitude lower than the solutions of Nicastro or Rasmussen. In this “Galactic Halo” solution, the O VI is not cospatial, as argued by Savage et al. (2005) and Williams et al. (2005), but might arise nearby as the O VII gas cools and recombines or if there is a conductive interface in a HVC.

The “Local Group” and “Galactic Halo” models represent limiting cases. The hot gas cannot be too small (e.g., in the disk) or it would overproduce the soft X-ray background. Also, the absorbing region cannot be larger than the virial radius of the Local Group or the gas would not have a potential well to fall into and become heated. To distinguish between these possibilities, one can search for an angular signature to the absorption line strengths. In particular, for a Local Group model, the absorption should be more pronounced for sight lines closer to the Milky Way - M31 axis. For a Galactic Halo model, the absorption should be more pronounced for sight lines across the Galaxy, compared to those away from the galaxy. Searching for such signatures requires a statistically significant number of sightlines with measured X-ray absorption lines, and for this purpose, the O VII resonance absorption line is the easiest to detect. There are relatively few *Chandra* observations of this line toward bright sources, in part because the gratings are not frequently used (but they have still proven quite useful; McKernan et al. 2004; Fang et al. 2006; Yao & Wang 2005; Wang et al. 2005). However, for *XMM* observations, the combination of the spectrograph (*RGS*) always operating plus the larger collecting area has led to a significant number of viable targets for O VII absorption measurements. Here we present the sample of the brightest AGNs that have been observed by *XMM* and were available through the archive as of April 2006. We show that this sample leads to a compelling case for the Galactic Halo model of X-ray absorbing gas.

2. Object Selection and Data Analysis

We wish to sample a path length as large as the Local Group, which implies the selection of extragalactic sources, with AGNs being the most suitable. The only AGNs that can be used for X-ray absorption line studies are bright and have been observed for a sufficiently long time. We constructed a list of the brightest AGNs from the archival data obtained by *ROSAT* and *ASCA*. This is a valuable starting point, but AGNs are variable, so some sources that were fainter in the past can be brighter now. Therefore, using the archive, we inspected the *XMM-Newton RGS* data for dozens of targets and chose the most suitable objects. The quantitative goal was to find sources for which the resulting uncertainty in the

O VII equivalent width is about 10 Å or less, since the typical absorption line strength was seen to be about 20 Å in previous studies. This led to a sample of 25 AGNs, plus we also included a source in the LMC, LMC X-3 (Table 1).

Many of these sources have been observed multiple times over the lifetime of XMM and so the data can be combined to improve the signal-to-noise. Unfortunately CCD 4 in the RGS2 failed shortly after launch and since it covers the wavelength range 20.1–23.9 Å only the RGS1 data is useful. The data was reduced in the usual manner, using the XMM SAS software (version 6.5), and was cleaned using an iterative three sigma clipping of a lightcurve from a background region on CCD 9, to remove periods of high background that would degrade the signal-to-noise. First order source and background spectra were produced from the cleaned events using the SAS task RGSSPECTRUM and response matrices were generated using RGSRMFGEN. The RGS1 first order spectra from the observations of each source were background subtracted, and after each spectrum was corrected for the effective area, they were combined to produce a single spectrum for each source. We note that the instrumental redistribution of photons in channel space is not corrected for. This is considered below.

To fit absorption lines, we excluded regions of known detector features and regions of intrinsic AGN absorption and emission lines. For the O VII resonance line at 21.603 Å, there is a detector feature at about 21.82 Å when the data are reduced with the standard SAS, so the 21.77–21.84 Å region was excluded in the fits (blank regions in our figures). Many of these bright objects are nearby Seyfert galaxies, which have their own O VII lines, some of which occur in absorption and some in emission. In most cases, the lines are sufficiently redshifted that they do not contaminate the local O VII absorption, but they restrict the region redward of 21.6 Å that can be used to define the baseline. The redshifted lines are marked on the figures of the spectra when relevant: MCG-6-30-15, Mkn766, NGC 3783, NGC 4051, NGC 5548, NGC 3516, NGC 4593, and IC4329a (Figures 1-6). In the few cases where there are no useful continuum regions redward of 21.6 Å, we used a flat continuum to the blue side of the line. There were objects for which the intrinsic absorption or emission line is badly blended with the Galactic O VII absorption line, such as NGC 4151. Although it is suitably bright, it has a broad O VII resonance emission line that overlaps with the $z = 0$ O VII feature. The local absorption line, although present, lies in the sharply rising wing of the NGC 4151 emission line, so the equivalent width of the absorption feature cannot be measured reliably. NGC 4151, and other similar objects were not included in the sample.

When there are no intrinsic AGN features near 21.6 Å, we fit a linear continuum in the range 21.2 - 21.96 Å, the upper limit being set by the need to avoid Galactic O VI $K\alpha$ absorption at 22.05 Å (Pradhan et al. 2003). In addition to the continuum, we fit a Gaussian

absorption line for the Galactic O VII absorption feature. The least-squares minimization has been performed by both the Simplex method and using a Levenberg-Marquardt minimization and we arrive at the same result. In practice, there are five parameters in this model: the continuum level; the slope of the continuum; the central wavelength of the absorption line; the Gaussian σ of the absorption line; and the area of the line (the line depth), which can be negative or positive (absorption and emission are permitted). Certain constraints can be applied to some of these parameters. For example, the Gaussian fit cannot be narrower than the instrumental width ($\sigma = 0.03 \text{ \AA}$ or $\text{FWHM} = 0.06 \text{ \AA}$) and it probably will not be wider than a velocity corresponding to the escape velocity of the Local Group, which we estimate to be about 700 km s^{-1} , or $\sigma = 0.05 \text{ \AA}$. Similarly, the location of the line center should not be outside of sensible Local Group velocities, which sets a displacement of about 500 km s^{-1} , or 0.036 \AA . In carrying out our fits, we calculate an uncertainty for each parameter. Only in a few cases are the uncertainties for the line center and line width smaller than the allowed range, and for the five highest S/N sources, Mkn 421, PKS 2155-304, 3C273, MCG-3-30-15, and LMC X-3, the median values of the central wavelength and line width are 21.605 \AA and $\sigma = 0.081 \text{ \AA}$, with small ranges. Consequently, for fainter sources where the central wavelength and line width cannot be accurately determined, we fix the central wavelength at 21.603 \AA and the line width at $\sigma = 0.08 \text{ \AA}$. When we relax these constraints, the values for the equivalent widths do not vary greatly, although the uncertainty will naturally be larger. We note that the uncertainty determined from photon counting statistics for the bins of the combined spectra appear to overestimate the true rms since the least square fits have a χ^2 that is too small (one can verify this by inspection in that a fit goes through nearly every error bar). To achieve a typical χ^2 for an acceptable fit, we estimate that the uncertainty per point would need to be reduced by 25-80% , depending on the object. This is due to a misalignment between the raw channels and the flux binning, introduced in the creation of the combined spectra, resulting in a lack of independence between adjacent flux bins. To verify that neither the non-independence of the flux bins nor the lack of treatment of the instrumental redistribution are significantly affecting our results, we have simultaneously fitted the individual spectra in XSPEC for some test cases.

Upon examining the spectra, there were no absorption features that deviated from expectations, with the exception of NGC 7469, where there is a possible absorption feature at -900 km s^{-1} (98% confidence), a velocity shift is much greater than the instrumental uncertainty. However, with 26 objects, there is a near-unity chance of finding one such feature over a range of $\pm 1000 \text{ km s}^{-1}$, so we do not consider this a real detection.

The resulting line strengths and statistical uncertainties are given in Table 2 and the spectra are given in Figures 1-6. The objects are ordered by decending values of their continuum S/N, which is a figure of merit for the quality to which uncertainties on the equivalent

widths can be obtained. Of the 26 objects, 10 have detections above a 3σ threshold, six are at the $2\text{--}3\sigma$ level and the remainder are below 2σ . Even non-detections are important, provided that the uncertainties are adequately small. For this sample, 18 objects have uncertainties to the equivalent widths of 10 \AA or less, and this forms the most useful subset of our data. There happens to be a decrease in quality of the spectra after object 18, but we also have used the remaining objects in some tests (although as those tests are weighted by the errors, these last eight objects do not have a large influence on the results).

A few sources were observed with both *XMM* and *Chandra*, and in nearly every case, the *XMM* data is of higher S/N. The exception is the source LMC X-3, where the *XMM* and *Chandra* data (Wang et al. 2005) are of comparable S/N and their equivalent widths are nearly identical. The line strengths measured by others for the *XMM* data give very similar results (e.g., Rasmussen et al. 2007), the differences being consistent with different fitting methods. Other approaches to fitting the same data (e.g., within XSPEC or IRAF) yielded nearly identical results.

There are other, weaker absorption lines present, although there are not enough of them to form a useful set for angular studies. The most relevant is the O VIII $K\alpha$ line, which can be used with the O VII $K\alpha$ line to constrain the temperature. The only useful objects are Mkn 421, PKS 2155-304, and 3C273, reported on by Rasmussen et al. (2003), so we use their results for the O VIII to O VII line ratios.

3. Analysis of the Data

The primary goal is to determine whether the absorption lines have an angular signature that correlates with either the Local Group structure, or various Milky Way properties. Given the limits of the data, it is impractical to fit multi-parameter models to the data, so we choose simple representative models, although we have explored a wide range of models.

3.1. Local Group Models

We begin with the model for the Local Group, and as there are no widely accepted models for the distribution of diffuse hot gas, here we assume that the diffuse baryons are aligned along the axis defined by the Milky Way and M31, which are the two dominant mass components of the Local Group. If the center of mass of the diffuse baryons lies halfway between M31 and the Milky Way, then the greatest column density should occur in a sightline toward M31 and the smallest column would occur in the anti-M31 direction.

Consequently, a general test is whether the column density decreases with increasing angle from M31. This prediction is not confirmed by the data (Figure 7), where the equivalent widths weakly increase with increasing angle from M31, rather than decrease.

With a more detailed model, one can predict the expected distribution of the column densities for comparison to the data. The specific model that we adopt is where M31 and the Milky Way lie at the two foci of an ellipsoid in which the gas density is uniform. The model is completely defined by choosing a semi-major axis, and we show the results for a model where the semi-major axis is twice the separation between M31 and the Milky Way (semi-major axis of 1.54 Mpc). The normalization of the column density of the model is a remaining parameter, which we choose to minimize the χ^2 . Inspection of the model fit (Figure 8) indicates it is a poor fit, and as the reduced $\chi^2 = 5.5$, it is an unacceptable fit. For semi-major axis from 0.8-2 Mpc, all models produce unacceptable fits with no positive correlation coefficients, showing that it is unlikely that the O VII-absorbing gas is distributed through the Local Group.

We have also compared the location of the absorbers with the individual Local Group galaxies to determine if they have a specific signature. For example, if individual galaxies were to have their own extended gaseous halos, there would be stronger absorption lines for sight lines near those galaxies (Figure 9). If galaxy gaseous halos scale with galaxy size, then the largest external galaxy halo should be around M31, where the closest sightline is Akn 564, 29° away, or a closest approach of 380 kpc. The equivalent width in this sight line (12.3 ± 4.6 mÅ) appears to be less and is certainly not substantially greater than the median equivalent width. This implies that if M31 has a significant gaseous halo, it is less than 380 kpc in radius.

The next largest galaxy with a nearby sightline is M33, where 3C 59 is 9° away, or a 130 kpc impact parameter. The O VII equivalent width, 60.9 ± 19.2 mÅ, has a rather large uncertainty, so it is difficult determining whether there a hot halo exists around M33. Two dwarf galaxies have nearby sightlines: DDO 210, where Mrk 509 is 3° away (42 kpc); and Leo I & II, where Ton 1388 is 3.5° away (14 kpc). The equivalent width for Ton 1388 is above average but fairly uncertain, 34.5 ± 15.7 mÅ, and is within 1σ of the median value for the sample. For Mrk 509, the detection is quite good (25.9 ± 7.3 mÅ) and it also is within 1σ of the median value. So for Leo I & II, there appears to not be a gaseous halo either, although this dwarf pair does not have HI nor does it have star formation (Mateo 1998). The observations, which are only of high quality for M31 and Leo I & II, argue against substantial halos with a size an order of magnitude larger than the optical galaxy. The data do not rule out smaller galactic halo that are comparable or a few times larger than the host galaxy.

There is one useful source within the LMC, LMC X-3 and it lies in the disk, 6.9 deg (6.7 kpc) from the center of the LMC. If a LMC halo surrounds the galaxy, this sightline would sample half of the LMC halo plus the intervening gas between it and the Sun. The source LMC X-3 has an equivalent width that is very close to the median value (21.0 ± 5.0 mÅ) and the line width is no wider than average (0.063 ± 0.012 Å), so there is no indication of additional absorption toward this source caused by a LMC halo. Finally, the line center (21.592 ± 0.016 Å) is consistent with the velocity of the Milky Way, but 2σ lower in redshift than the LMC, which would have produced a line at 21.623 Å. This is similar to the conclusions of Wang et al. (2005), who used *Chandra* data to observe LMC X-3.

3.2. Galactic Halo Models

Another model that we consider is for a hot Galactic Halo, where the simplest assumption is that a hot gas halo is centered on the Galaxy center. In this picture, the column density of hot gas should be a decreasing function of angle away from the Galactic center, and as shown in Figure 10, there appears to be the expected inverse correlation. An unweighted linear y-on-x fit shows that there is an inverse correlation with angle at the 95% confidence level, supporting the Galaxy Halo model. To be more quantitative, yet to keep the model simple, we calculate relative column densities for a uniform sphere of radius R_H , which is the only free parameter (the equivalent width is constrained to be zero for zero path length); we use 8.5 kpc as the distance of the Sun from the center of the Galaxy. A fit of similar significance is found (Figure 11), where a best-fit χ^2 model leads to $R_H = 20.6$ kpc, and the 95% confidence bounds are 15-110 kpc. For the best-fit model, the χ^2 is unacceptably large, which can occur if the statistical uncertainty in the equivalent widths are smaller than the variation due to structure in the absorbing medium. To obtain an acceptable value of χ^2 , we added an intrinsic scatter in the equivalent widths attributable to the structure of the absorbing gas of 4 mÅ, or 23% of the median value of the equivalent width.

The above model represents a spherical halo where the density $n \propto r^0$, but we can also consider models where the density is a decreasing function of radius, such as $n \propto (1 + (r/r_c)^2)^{-3\beta/2}$, where r_c is the core radius. The value of r_c in most other galaxies with hot gas is less than 1 kpc, which is significantly smaller than the radius of closest approach for all objects in the sample. Therefore, the value of r_c is not relevant for our sample and we can write the density function as a power-law, $n \propto r^{-3\beta}$, and we choose to examine $n \propto r^{-3/2}$, as this is similar to that found for the hot gas in ellipticals ($\beta=1/2$ in the “beta” models used for ellipticals, e.g., O’Sullivan et al. 2003). While this leads to a gas mass that increases with radius as $r^{3/2}$ and an emission measure that increases logarithmically with radius, the

column density is convergent at large radius. There is only a modest correlation between the theoretical and observed equivalent widths, significant at the 92% confidence level (Figure 12). This model is closely associated with the Galaxy as well. From the available data, we cannot distinguish between the uniform model and this “beta” model. More complicated models can certainly be constructed, but given the quality of the data, we do not believe it is warranted at this time.

If this absorption is associated with a Galactic Halo, it might be correlated with the soft X-ray background of the Galaxy. The 1/4 keV X-ray background is dominated by the gas within a few hundred pc of the Sun, plus a flattened hot halo of height 2 kpc (Snowden et al. 1997). This is not the X-ray emission that we expect the absorption features to be related to and there is no correlation between the 1/4 keV surface brightness and the O VII equivalent widths. At higher energies, such as the 3/4 keV band, the emission is a mixture of emission from hot Galactic gas plus emission from unresolved AGNs (Gilli et al. 2001). Also, the absorption of the X-rays by neutral Galactic gas is less of a problem at these energies. It is probably the best energy at which to detect diffuse Galactic emission and it has been known that there is enhanced soft X-ray emission in the general direction of the bulge (Snowden et al. 2000). A correlation exists between R45 and the O VII equivalent width at the 99% confidence level (weighted or unweighted fit), without requiring that the fit go through the origin (Figure 13). This relationship is better than the correlation found with angle from the Galactic Center or with either of the above Galactic Halo models. For this fit, the $\chi^2 = 45$ (16 dof), which is unacceptable at the 99% confidence level, so we added a additional rms in the equivalent width, as described above. For an additional rms of 3.5 mÅ (19% of the median equivalent width), the χ^2 is reduced to an acceptable 28.5 and the probability of a weighted fit is reduced to the 98% confidence level. The high initial χ^2 is due to one low point and if this outlier were removed, the quality of the fit would improve. By using the entire sample and creating error-weighted bins (Figure 14), we obtain a similar level of significance, although a somewhat lower additional rms is required in this case (3.0 mÅ) to obtain acceptable values of χ^2 .

The R45 band emission contains not only large-scale Galactic emission, but individual bright features due to multiple supernovae, such as the North Polar Spur. We examined the location of the objects to determine if they lie in bright regions of these features, but there are hardly any coincidences. The quasar 3C273 is located near a fainter part of the North Polar Spur, but its O VII equivalent width is not remarkable (24.6 ± 3.3 mÅ). The strongest component of the R45 emission is the O VII emission triplet, so the relationship between the R45 emission and the absorption equivalent widths suggests a correlation between the O VII emission and absorption. This implies that the O VII emission and absorption is largely cospatial.

Another piece of evidence for the Galactic Halo picture is the mean redshift of our four highest S/N AGNs. There is a random uncertainty in the wavelength calibration of 0.008 \AA (XMM-Newton Users’s Handbook), or 111 km s^{-1} , so it is helpful to average together several objects. Using these four AGNs, the unweighted mean central wavelength is 21.608 \AA ($+70 \text{ km s}^{-1}$), and the inferred standard deviation of a single point is 0.006 \AA , but to be conservative, we assume that it is 0.010 \AA , as this is the median value for the uncertainty in the central wavelength from individual fits. Then, the uncertainty in the mean central wavelength is 0.005 \AA (55 km s^{-1}), which places this mean about 1σ of the Milky Way ($z = 0$, or 21.603 \AA). The Local Group is probably at -250 km s^{-1} , a wavelength of 21.585 \AA , 4.6σ different from the measured mean value. This suggests that the absorption is most likely associated with the Milky Way and not the Local Group.

The conversion of the O VII equivalent width to a hydrogen density, which will yield a length scale as well, requires knowledge of the oxygen column density, the oxygen abundance, and the fraction of oxygen in the form of O VII. When the optical depth of the absorption line is low, there is a simple linear relationship between the equivalent width and the column density, $N(\text{O VII}) = 3.48 \times 10^{14} \text{ EW}$, where the equivalent width (EW) has units of m\AA and the column density, $N(\text{O VII})$ has units of cm^{-2} . If the lines are resolved or if the gaseous medium is turbulent at the sound speed, then the optical depth is small, but if the lines have a Doppler width for oxygen (no turbulent or significant ordered motion), the optical depth at the line center can be 0.1-0.4. As the optical depth rises, the higher order lines, such as O VII $K\beta$, become of equal strength to the $K\alpha$ line. We examined the strength of the $K\beta$ for the highest S/N spectrum, of Mkn 421, and find a value of $3.6 \pm 1.1 \text{ m\AA}$, although an instrumental feature contaminates the red side of the line. The $K\beta$ to $K\alpha$ ratio is 0.30 ± 0.11 , which is within 1σ of the ratio of the f values, 0.21. This is consistent either with a small or modest optical depth. Here we will calculate column densities in the limit of low optical depth.

The ionization fraction can be determined by forming the ratio of O VII with an adjacent ionization state, such as O VI or O VIII, provided that the different ionization states are cospatial. The relationship between O VII and O VI is poor and both Savage et al. (2005) and Williams et al. (2005) argue that the two are probably not closely related. It is tempting to relate O VIII to O VII, and a correlation between these two quantities would lend support to this possibility. Unfortunately, there are only a few objects for which we can determine useful measurements of O VIII absorption, the errors are significant, and there is no statistically meaningful correlation between the two quantities (Rasmussen et al. 2003). It is possible to have a multi-temperature medium where the hotter component leads to O VIII while a slightly cooler component dominates the O VII. As the above study showed that O VII emission and absorption are correlated, we will use these two measurements to

obtain densities and length scales, later considering whether it is consistent with the O VIII to O VII column density ratio.

For a Galactic Halo model, we expect the metallicity to be similar to the value in the ISM and the Sun. For oxygen, the “Solar” abundance has changed considerably in the past two decades and is still not a settled issue. The most commonly cited Solar abundances come from Anders & Grevesse (1989), where $\log N_{\text{O}} = 8.93$, but Holweger (2001) recommends a value of 8.736, a 35% reduction from the older value. Asplund et al. (2005) advocates a value at least 20% lower, but here we adopt the value 8.74 for the oxygen abundance. For an ion fraction $f = 0.5$, this leads to an electron column of $N_e = n_e L = 5.8 \times 10^{19} (N_{\text{OVII}}/10^{16} \text{ cm}^{-2}) (f/0.5)^{-1} \text{ cm}^{-2}$, where n_e is the electron density and L is the path length for a constant density slab. The emission measure is available from only one line of sight, toward $l, b = 90^\circ, 60^\circ$ and with a 1 sr field of view (McCammon et al. 2002). Toward this general location, R45 is typically 200 cnt s⁻¹ arcmin⁻², above the mean of the lines of sight we have studied. For sight lines at similar values of R45, the typical equivalent width is 25 mÅ, or a column density of $N_{\text{OVII}} = 8.7 \times 10^{15} \text{ cm}^{-2}$ and $N_e = 5.0 \times 10^{19} \text{ cm}^{-2}$. The emission measure at Solar metallicity is $\text{EM} = n_e^2 L = 0.009 \text{ cm}^{-6} \text{ pc}$ (McCammon et al. 2002), so one can use this, adjusted to our oxygen abundance, and the column density to solve for the length scale L , and we find $L = 19 \text{ kpc}$ and $n_e = 9 \times 10^{-4} \text{ cm}^{-3}$. This length scale supports the Galactic Halo model for the hot gas distribution. Aside from the temperature dependence, $L \propto f^{-2} (O/H)^{-1}$, so for $f = 1$, the halo could be as small as 5 kpc. A value smaller than 5 kpc is ruled out because it would have the consequence of raising the emission measure above the observed value.

The O VIII to O VII column density ratio is consistent with a gas whose temperature is $\log T = 6.2\text{-}6.3$. This column density ratio changes rapidly in this temperature range, so even a modest amount of temperature variation along the line of sight (e.g., 20-30%) can make a difference in this ratio by a factor of several, as Fang et al. (2006) points out. The analysis of the emission in the R45 band indicates a temperature of $\log T = 6.0\text{-}6.1$ (Snowden et al. 2000; McCammon et al. 2002), so the O VII absorption may also be occurring in a temperature a bit too low to produce the O VIII absorption as well. Temperature variation at this level is seen in some early-type galaxies (e.g., NGC 4636; Jones et al. 2002), and if a positive temperature gradient is present in the Milky Way halo, there could be radial regions where O VII is dominant and more distant regions where O VIII is dominant. A radial decomposition of the O VII to O VIII ionization fraction ratio is possible in principle, but the present data are inadequate for such work.

4. Summary and Final Comments

We sought to determine whether the X-ray absorption, primarily in the O VII resonance line, were due to a Local Group medium or a hot Galactic Halo. It is possible to address this question by searching for the spatial signature of these two models, which are distinct. The Local group is expected to be elongated along the axis defined by the Milky Way and M31. For our model, where the two galaxies are placed at the foci of an ellipsoid of rotation about the MW-M31 axis, the greatest column would result toward M31 and the smallest in the opposite direction. For the Milky Way Halo model where the halo is comparable to the size of the Galaxy, the greatest columns would occur when looking across the Galaxy, in the general direction of the bulge. By good fortune, these two models are nearly orthogonal in that the minimum direction for the Local Group model, the anti-M31 direction, is at $l, b = 301^\circ, 21.6^\circ$, where the Galactic Halo model would predict an excess compared to the mean sightline.

The comparison between the absorption line data and the models shows that the Galactic Halo model is preferred. The data do not permit us to accurately determine the properties of the halo so we adopted the simplest possible model, a uniform spherical halo. In the context of this model, the characteristic radial size lies in the range 15-100 kpc. The redshift of the lines is consistent with a Galactic origin rather than a Local Group origin. The absorption line data correlates best with the R45 (0.4-1 keV) emission, for which the biggest contribution is the O VII emission triplet. This suggests that the O VII emission and absorption are cospatial to some degree, and for a cospatial model, we derive an independent measure of the size of the halo, which is about 20 kpc. Constraints on the temperature may be provided by using the O VIII absorption as well, which leads to a temperature of $\log T = 6.1$, as discussed previously (McCammon et al. 2002; Fang et al. 2006). These results are in good agreement with the work of Fang et al. (2006), who also argue for a Galactic origin based on *Chandra* observations and on the absence of X-ray absorption by other groups.

As an example of a possible halo, when we consider a uniform Galaxy halo of radius 20 kpc, the mass for the hot gas is about $4 \times 10^8 M_\odot$, which is considerable, but only a small fraction of the gaseous content of the Galaxy, and orders of magnitude less than the values suggested for the Local Group models (Nicastro et al. 2002). This amount of mass is similar to that found in the less X-ray luminous early-type galaxies, and it is comparable to the amount of mass suggested to be present due to Galactic Fountain models (Rosen & Bregman 1995; de Avillez & Breitschwerdt 2004). Also, this mass is much less than the external baryon mass predicted by in some N-body/gasdynamical simulations (Sommer-Larsen 2006), which is expected to be comparable to the baryonic mass of the disk plus bulge stars and the gas in the Galaxy ($5 \times 10^{10} M_\odot$). While we have assumed a Solar-like metallicity, we note

that the oxygen abundance cannot be significantly lower, as it would lead to a higher electron column density that would exceed the values determined from the dispersion measure toward pulsars. At the pole, the pulsar dispersion measure implies an electron column of $5.1 \times 10^{19} \text{ cm}^{-2}$ (Taylor & Cordes 1993), comparable to the column inferred from the O VII. Already, there is hardly room for the contribution from the 10^4 K gas that is known to exist around the disk (Reynolds 2004), so any decrease in the oxygen abundance or the O VII fraction can be excluded. The constraint provided by the pulsar dispersion measure argues for near-Solar abundances and an O VII ionization near unity.

A weak limit on the size of hot halos around other galaxies is provided by the failure to find enhanced absorption toward M31, where the sightline of the nearest object passes 380 kpc from its center. Also, there was no substantial enhancement in the O VII (or O VIII) absorption toward LMC X-3, which suggests that there is not a significant 10^6 K halo around the LMC. This is consistent with the results of Wang et al. (2005), who showed that the redshift of the line center, as determined with *Chandra*, is inconsistent with an LMC origin and consistent with a Galactic origin. A cooler ionized halo is known to exist around the LMC, which is responsible for the enhanced dispersion measure toward pulsars (Manchester et al. 2006).

This study does not rule out some component of the O VII emission lying in a Local Group medium. Certainly, the Local Group is not devoid of gas, so it must have some O VII as well. However, as Fang et al. (2006) discuss, if galaxy groups commonly had a significant O VII column, it would be detected in sight lines toward background AGNs at a rate in conflict with existing limits.

There is more work that can be carried out with *XMM* data, as new observations are improving the S/N for some AGNs and additional AGNs are being observed for significant amounts of time. However, *XMM* and *Chandra* will not be able to provide us with $\sim 10^2$ sight lines with high S/N line measurements, which would be needed to map out the structure of the hot halo, much in the same way as has been accomplished for lower temperature gas with *IUE*, *HST*, and *FUSE* spectra. An improvement in the X-ray capabilities of an order of magnitude would provide the necessary data, and this will become possible with *Constellation-X*.

The authors would like to thank Andy Rasmussen, Wilt Sanders, Jimmy Irwin, and Renato Dupke for their comments and insight. We are indebted to those who have developed and maintained the XMM archive, upon which this work was based. Also, we would like to acknowledge support from NASA for these activities, through the Long Term Space Astrophysics grant NAG5-10765, and also NAG5-13137.

REFERENCES

- de Avillez, M., & Breitschwerdt, D. 2004, *Ap&SS*, 292, 207
- Anders, E., & Grevesse, N. 1989, *Geochim. Cosmochim. Acta*, 53, 197
- Asplund, M., Grevesse, N., & Sauval, A. J. 2005, *ASP Conf. Ser.* 336: *Cosmic Abundances as Records of Stellar Evolution and Nucleosynthesis*, 336, 25
- Braun, R. 1991, *ApJ*, 372, 54
- Cagnoni, I., Nicastrò, F., Maraschi, L., Treves, A., & Tavecchio, F. 2003, *New Astronomy Review*, 47, 561
- Carignan, C., Chemin, L., Huchtmeier, W. K., & Lockman, F. J. 2006, *ApJ*, 641, L109
- Cox, A. N. 2000, *Allen's astrophysical quantities*, 4th ed. Publisher: New York: AIP Press; Springer, 2000. Edited by Arthur N. Cox. ISBN: 0387987460
- Fang, T., Croft, R. A. C., Sanders, W. T., Houck, J., Davé, R., Katz, N., Weinberg, D. H., & Hernquist, L. 2005, *ApJ*, 623, 612
- Fang, T., Mckee, C. F., Canizares, C. R., & Wolfire, M. 2006, *ApJ*, 644, 174
- Fox, A. J., Savage, B. D., Wakker, B. P., Richter, P., Sembach, K. R., & Tripp, T. M. 2004, *ApJ*, 602, 738
- Gilli, R., Salvati, M., & Hasinger, G. 2001, *A&A*, 366, 407
- Holweger, H. 2001, *AIP Conf. Proc.* 598: *Joint SOHO/ACE workshop "Solar and Galactic Composition"*, 598, 23
- Jones, C., Forman, W., Vikhlinin, A., Markevitch, M., David, L., Warmflash, A., Murray, S., & Nulsen, P. E. J. 2002, *ApJ*, 567, L115
- Mateo, M. L. 1998, *ARA&A*, 36, 435
- Manchester, R. N., Fan, G., Lyne, A. G., Kaspi, V. M., & Crawford, F. 2006, *ApJ*, 649, 235
- McCammon, D., et al. 2002, *ApJ*, 576, 188
- McKernan, B., Yaqoob, T., & Reynolds, C. S. 2004, *ApJ*, 617, 232
- Nicastrò, F., et al. 2005, *ApJ*, 629, 700

- Nicastro, F., et al. 2005, *Nature*, 433, 495
- Nicastro, F., et al. 2002, *ApJ*, 573, 157
- O’Sullivan, E., Ponman, T. J., & Collins, R. S. 2003, *MNRAS*, 340, 1375
- Paerels, F. B. S., & Kahn, S. M. 2003, *ARA&A*, 41, 291
- Pradhan, A. K., Chen, G. X., Delahaye, F., Nahar, S. N., & Oelgoetz, J. 2003, *MNRAS*, 341, 1268
- Rasmussen, A., Kahn, S. M., & Paerels, F. 2003, *ASSL Vol. 281: The IGM/Galaxy Connection. The Distribution of Baryons at $z=0$* , 109
- Rasmussen, A. P., Kahn, S. M., Paerels, F., Herder, J. W. d., Kaastra, J., & de Vries, C. 2007, *ApJ*, 656, 129
- Reynolds, R. J. 2004, *Advances in Space Research*, 34, 27
- Rosen, A., & Bregman, J. N. 1995, *ApJ*, 440, 634
- Sanders, W. T., et al. 2002, *Bulletin of the American Astronomical Society*, 34, 1178
- Savage, B. D., Wakker, B. P., Fox, A. J., & Sembach, K. R. 2005, *ApJ*, 619, 863
- Sembach, K. R., et al. 2003, *ApJS*, 146, 165
- Snowden, S. L., et al. 1997, *ApJ*, 485, 125
- Snowden, S. L., Freyberg, M. J., Kuntz, K. D., & Sanders, W. T. 2000, *ApJS*, 128, 171
- Sommer-Larsen, J. 2006, *ApJ*, 644, L1
- Taylor, J. H., & Cordes, J. M. 1993, *ApJ*, 411, 674
- van den Bergh, S. 2000, *The galaxies of the Local Group*, by Sidney Van den Bergh. Published by Cambridge, UK: Cambridge University Press, 2000 Cambridge Astrophysics Series Series, vol no: 35, ISBN: 0521651816.,
- Wakker, B. P., et al. 2003, *ApJS*, 146, 1
- Wang, Q. D., et al. 2005, *ApJ*, 635, 386
- Williams, R. J., et al. 2005, *ApJ*, 631, 856
- Yao, Y., & Wang, Q. D. 2005, *ApJ*, 624, 751

Table 1. Absorption Line Targets: Basic Data

No.	Name	l (deg)	b (deg)	z	N_H (10^{20}cm^{-2})	t_{exp}^a (ksec)
1	Mkn 421	179.83	65.03	0.0300	1.38	509
2	PKS 2155-304	17.73	-52.24	0.116	1.71	723
3	3C 273	289.95	64.36	0.1583	1.79	451
4	MCG-6-30-15	313.29	27.68	0.0077	4.06	460
5	LMC X-3	273.57	-32.08	0.000927	4.74	126
6	1H1426+428	77.49	64.90	0.129	1.38	388
7	Akn 564	92.14	-25.34	0.0247	6.27	130
8	NGC 4051	148.88	70.09	0.0023	1.32	174
9	NGC 3783	287.46	22.95	0.0097	8.26	316
10	NGC 5548	31.96	70.50	0.0172	1.69	160
11	Akn120	201.69	-21.13	0.0327	12.2	112
12	PKS 0558-504	257.96	-28.57	0.137	4.39	168
13	Mkn766	190.68	82.27	0.0129	1.71	189
14	NGC 4593	297.48	57.40	0.009	2.31	115
15	3C 390.3	111.44	27.07	0.0561	4.24	123
16	NGC 7469	83.10	-45.47	0.0163	4.87	189
17	Mkn 509	35.97	-29.86	0.0344	4.11	75
18	3C 120	190.37	-27.40	0.033	11.1	129
19	NGC 3516	133.24	42.40	0.0088	3.05	260
20	Ton 1388	223.36	68.21	0.1765	1.28	110
21	1H 0414+009	191.82	-33.16	0.287	10.3	79
22	Mr2251-178	46.20	-61.33	0.064	2.70	65
23	IC 4329a	317.5	30.92	0.0161	4.42	136
24	Fairall 9	295.07	-57.83	0.047	3.19	33
25	MS0737.9+7441	140.27	29.57	0.315	3.54	86
26	3C 59	142.04	-30.54	0.1096	5.84	82

^aCleaned exposure time for the *XMM RGS*.

Table 2. OVII Absorption Line Measurements

No.	Name	AngleGC (deg)	AngleM31 (deg)	R12	R45	R67	F_λ	S/N	λ_c (Å)	2σ (mÅ)	EW (mÅ)	err (mÅ)	S/N
1	Mkn 421	114.97	97.42	1087	105	116	1.24E-02	48.9	21.602	0.069	11.8	0.8	14.1
2	PKS 2155-304	54.32	80.89	964	145	135	2.88E-03	26.5	21.605	0.081	13.7	1.9	7.4
3	3C 273	81.51	136.57	1374	189	132	1.43E-03	14.7	21.608	0.083	24.6	3.3	7.4
4	MCG-6-30-15	52.61	167.41	826	304	189	9.42E-04	11.2	21.617	0.081	32.6	6.8	4.8
5	LMC X-3	86.97	120.20	533	160	156	9.00E-03	8.9	21.592	0.063	21.0	5.0	4.2
6	1H1426+428	84.73	92.73	1084	124	114	7.74E-04	8.0	21.603	0.08	11.6	4.1	2.8
7	Akn 564	91.93	26.84	429	115	115	1.85E-03	7.4	21.603	0.08	12.3	4.6	2.7
8	NGC 4051	106.95	93.74	1118	115	118	7.20E-04	7.4	21.603	0.05	24.6	3.1	7.9
9	NGC 3783	73.97	167.24	510	143	118	3.52E-04	5.9	21.603	0.08	24.1	7.6	3.2
10	NGC 5548	73.54	110.02	1052	152	139	7.79E-04	5.7	21.603	0.08	7.0	6.8	1.0
11	Akn120	150.08	74.02	444	141	155	7.03E-04	5.6	21.603	0.08	-6.0	5.5	-1.1
12	PKS 0558-504	100.56	114.80	500	122	120	6.89E-04	5.1	21.613	0.05	21.7	7.8	2.8
13	Mkn766	97.60	108.70	887	112	112	8.33E-04	5.1	21.603	0.08	0.2	6.8	0.0
14	NGC 4593	75.61	144.07	861	201	153	9.46E-04	5.0	21.603	0.08	23.4	8.5	2.8
15	3C 390.3	108.99	49.55	512	138	125	4.24E-04	4.3	21.603	0.08	27.4	7.3	3.8
16	NGC 7469	85.17	39.15	406	100	117	6.96E-04	4.2	21.603	0.08	1.6	8.9	0.2
17	Mkn 509	45.42	75.49	743	220	147	6.23E-04	4.0	21.603	0.08	25.9	7.3	3.6
18	3C 120	150.85	62.46	466	111	117	2.81E-04	3.5	21.603	0.08	13.8	9.2	1.5
19	NGC 3516	120.39	64.94	831	113	118	9.04E-05	2.5	21.603	0.08	22.0	13.4	1.6
20	Ton 1388	105.66	114.48	1004	121	128	1.41E-04	2.3	21.603	0.08	34.5	15.7	2.2
21	1H 0414+009	145.03	62.68	612	141	144	1.66E-04	2.2	21.603	0.08	-3.1	14.8	-0.2
22	Mr2251-178	70.60	64.00	646	137	126	1.37E-04	1.8	21.603	0.08	39.8	19.6	2.0
23	IC 4329a	50.77	162.66	669	248	155	1.85E-04	1.7	21.603	0.08	33.8	19.3	1.8
24	Fairall 9	76.96	100.44	893	122	124	2.17E-04	1.7	21.603	0.08	31.1	16.5	1.9
25	MS0737.9+7441	131.98	54.35	548	112	116	1.30E-04	1.6	21.603	0.08	-13.9	20.7	-0.7
26	3C 59	132.77	20.73	493	128	115	9.22E-05	1.5	21.603	0.08	60.9	19.2	3.2

Note. — AngleGC is the angle from the Galactic Center; AngleM31 is the angle from M31; R12, R45, and R67 are the *ROSAT* soft X-ray background values in units of 10^{-6} cnt s^{-1} arcmin $^{-2}$; F_λ is the continuum flux at 21.60 Å in units of cnt s^{-1} Å $^{-1}$ cm $^{-2}$, followed by its S/N; λ_c the the line center of the OVII absorption; σ is the Gaussian parameter describing the OVII line width; and EW is the equivalent width of the line.

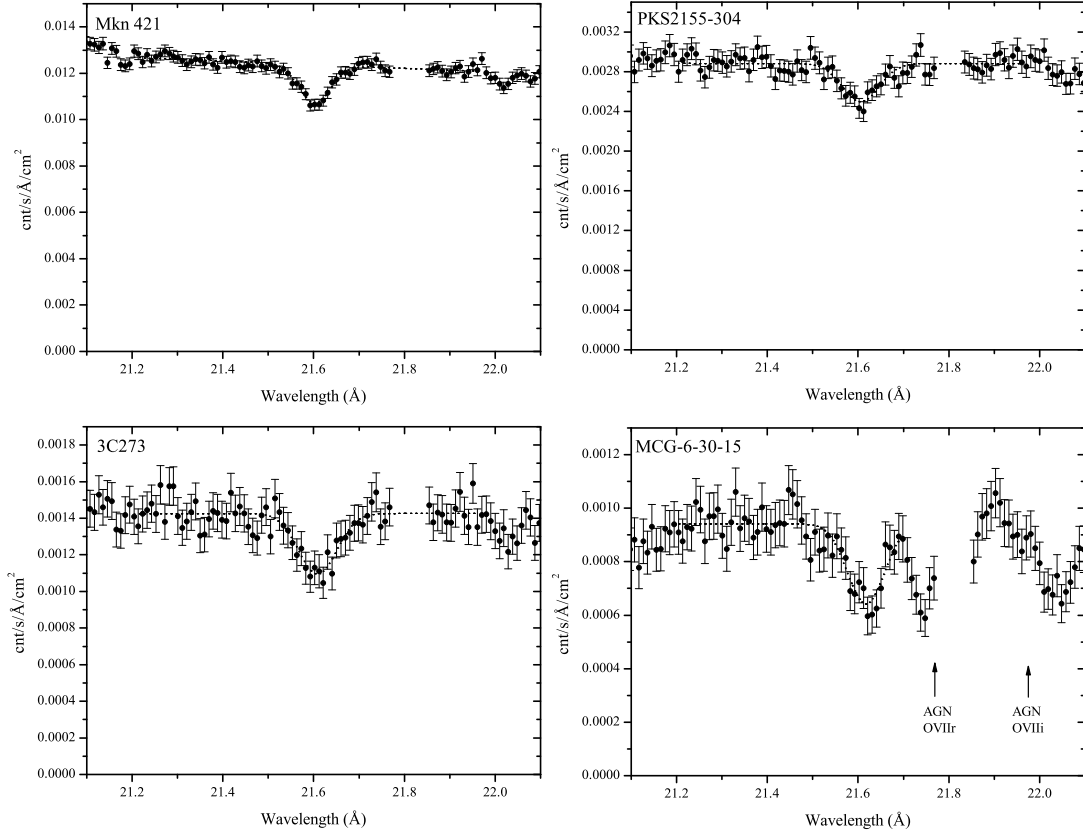


Fig. 1.— The *XMM* flux, corrected for instrumental features, at the location of the O VII line at 21.60 Å. There is an instrumental feature near 21.82 Å, which is not used in the fit; the fit is shown by the dotted line. A feature near 22.0 Å is from a Galactic O VI blend. The objects are shown by decreasing S/N of the continuum. For MCG-6-30-15, the location of the resonance and intercombination lines at the redshift of the object is shown.

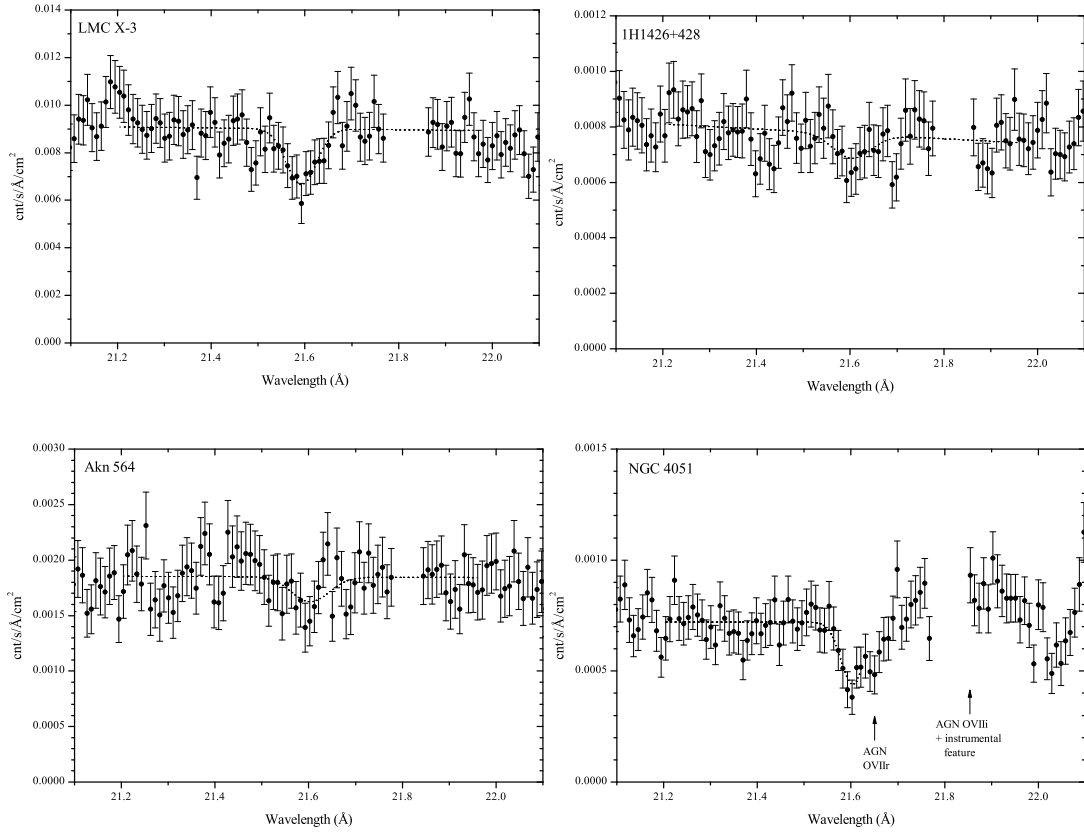


Fig. 2.— As above, where the objects are ordered by continuum S/N. The location of the AGN O VII lines in NGC 4051, if present are shown. For this source, the continuum is defined by the data blueward of the 21.60 Å line.

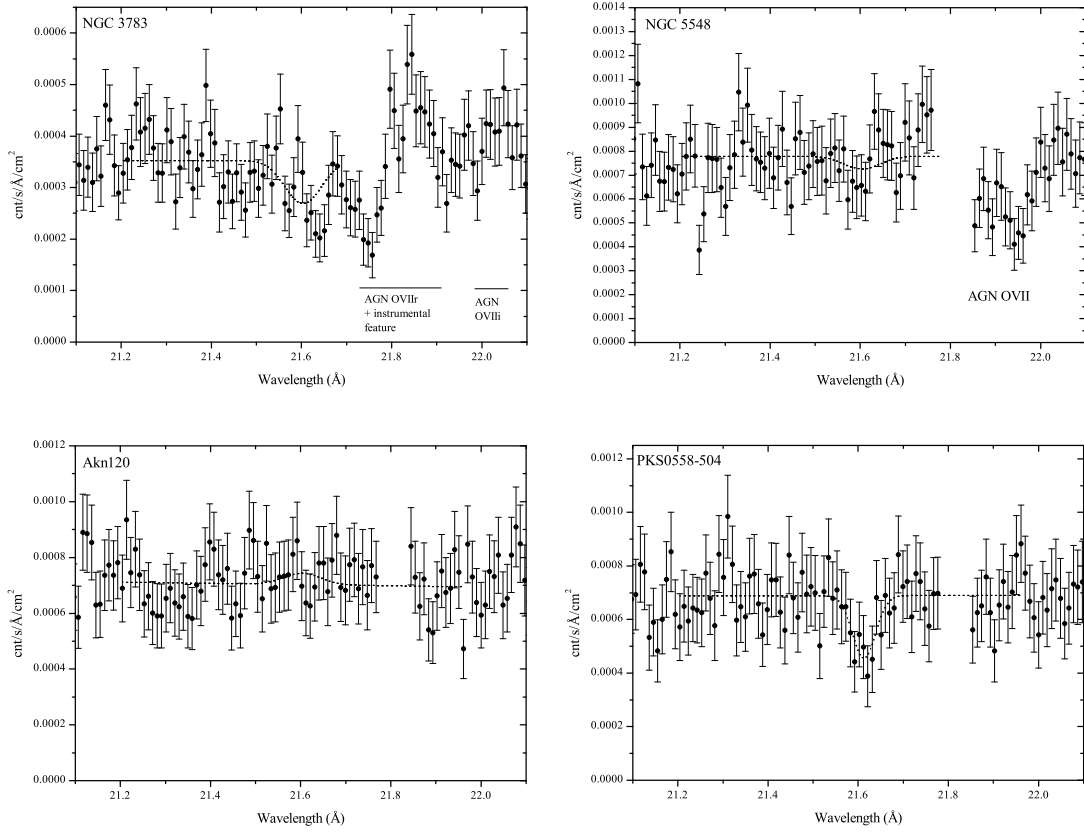


Fig. 3.— As above, for targets 9-12. NGC 3783 has a possible P Cygni profile in its redshifted resonance O VII line.

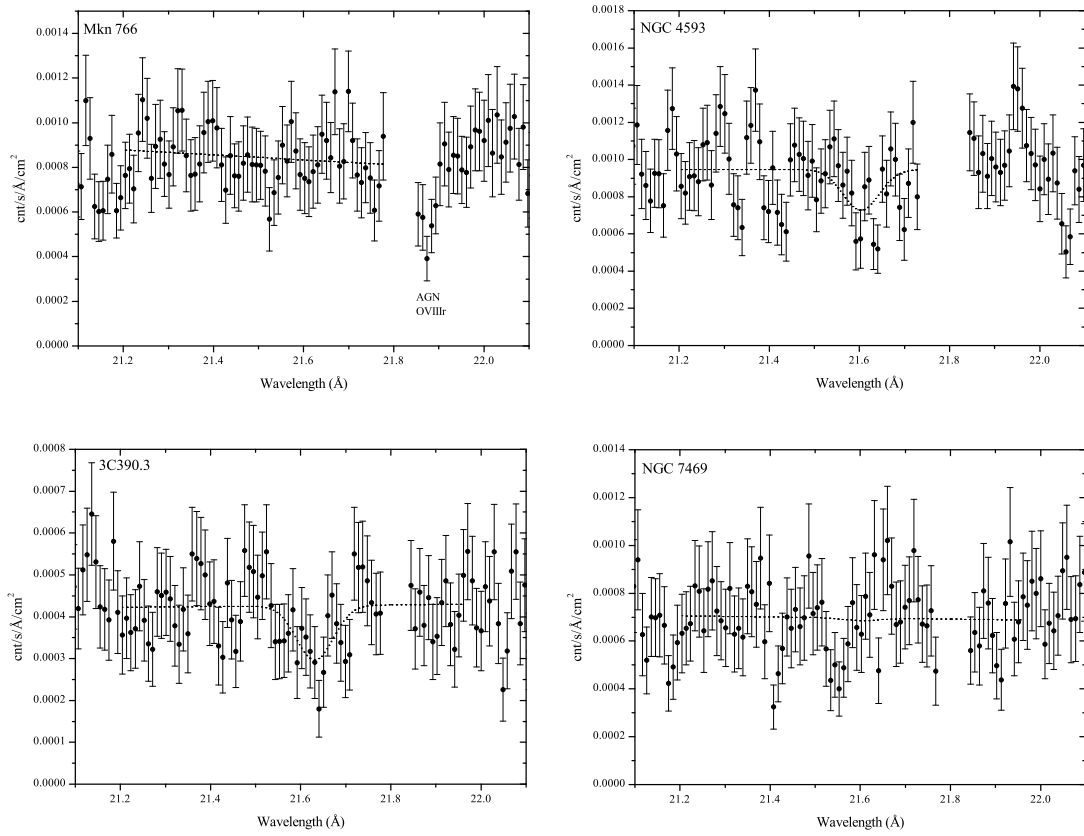


Fig. 4.— As above, for targets 13-16.

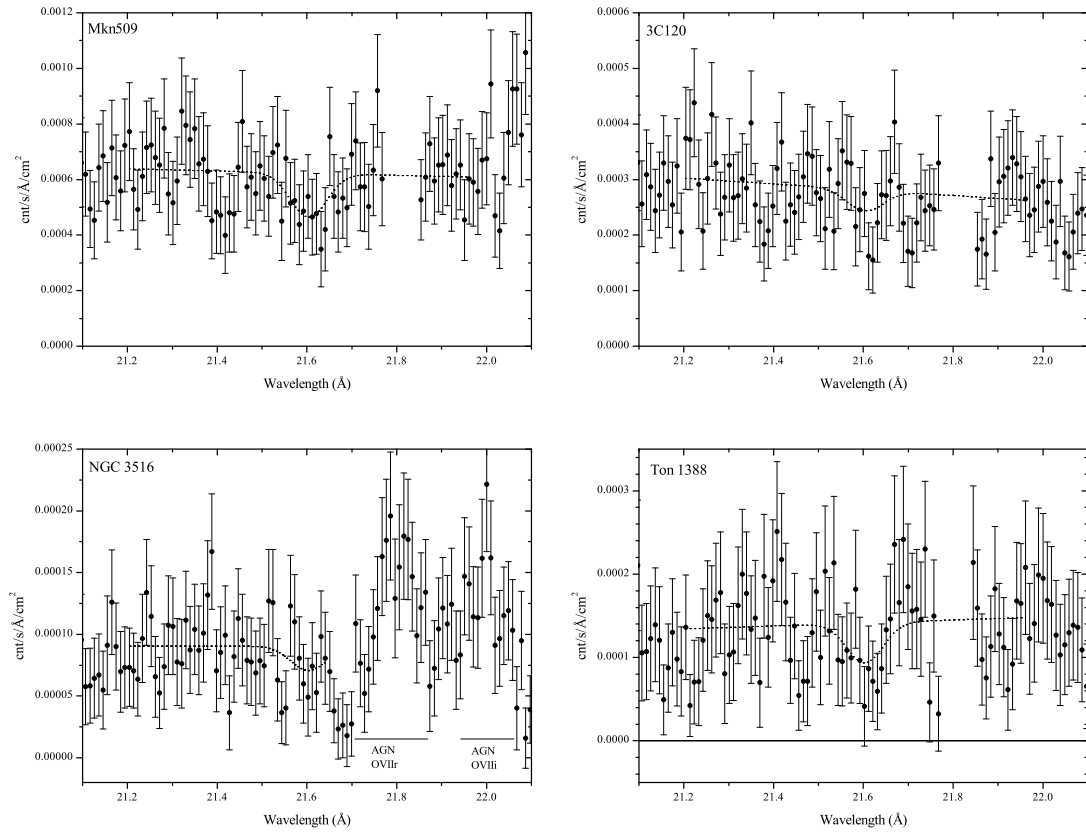


Fig. 5.— As above, for targets 17-20. For most of the analysis, we do not use targets 19 and higher and there is a decrease in S/N such that the uncertainty in the equivalent widths become too large. In NGC 3516, both the redshifted resonance and intercombination lines are present in emission.

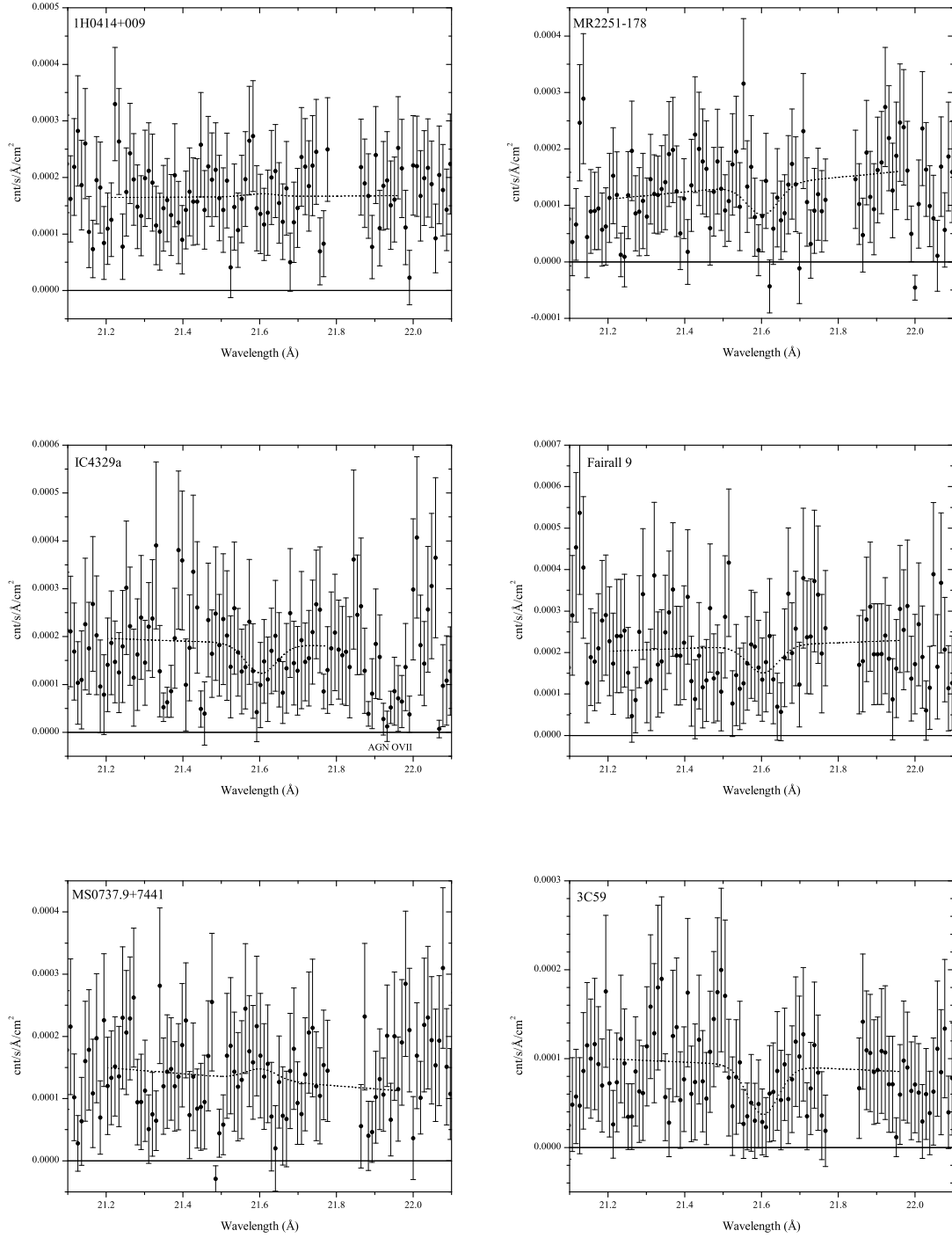


Fig. 6.— For these final six objects, the S/N is rather poor. The faintest source, 3C59, which shows possible absorption, lies within 130 kpc of M33.

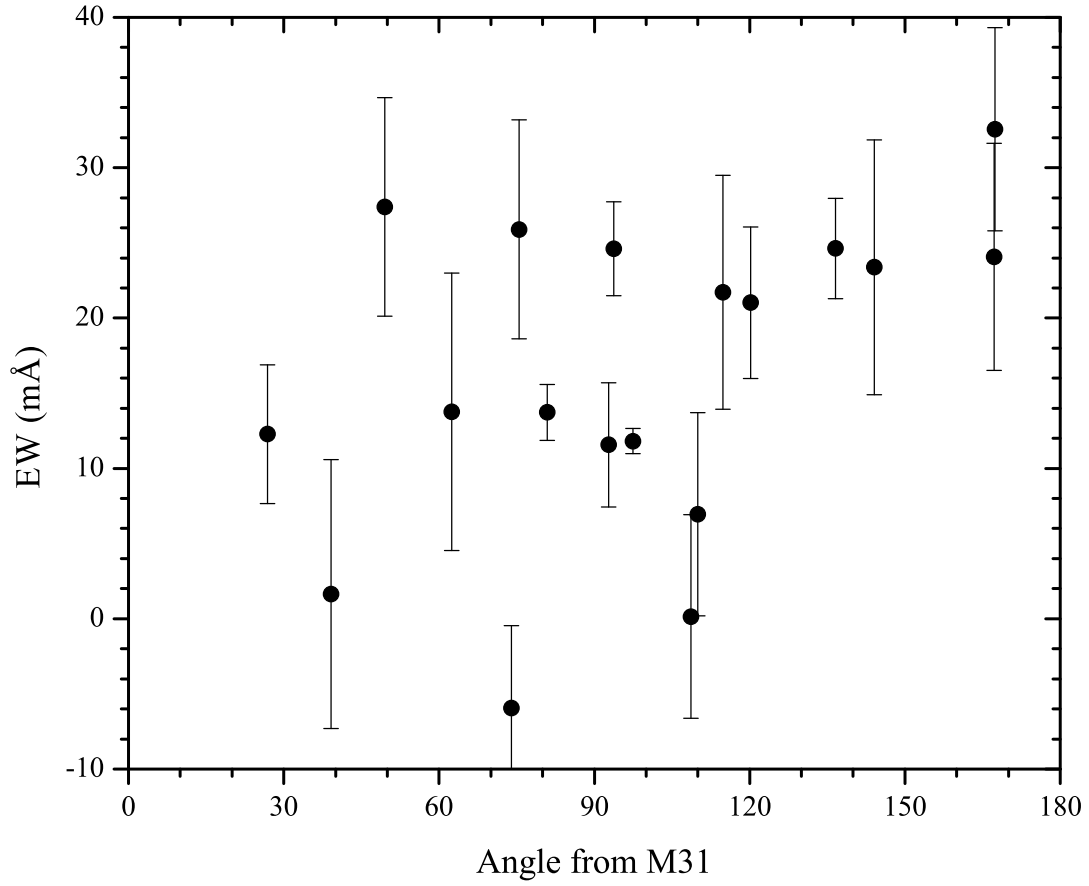


Fig. 7.— The distribution of O VII equivalent widths as a function of angle from M31. In the Local Group model, we would expect a decreasing equivalent width with increasing angle, a prediction not verified.

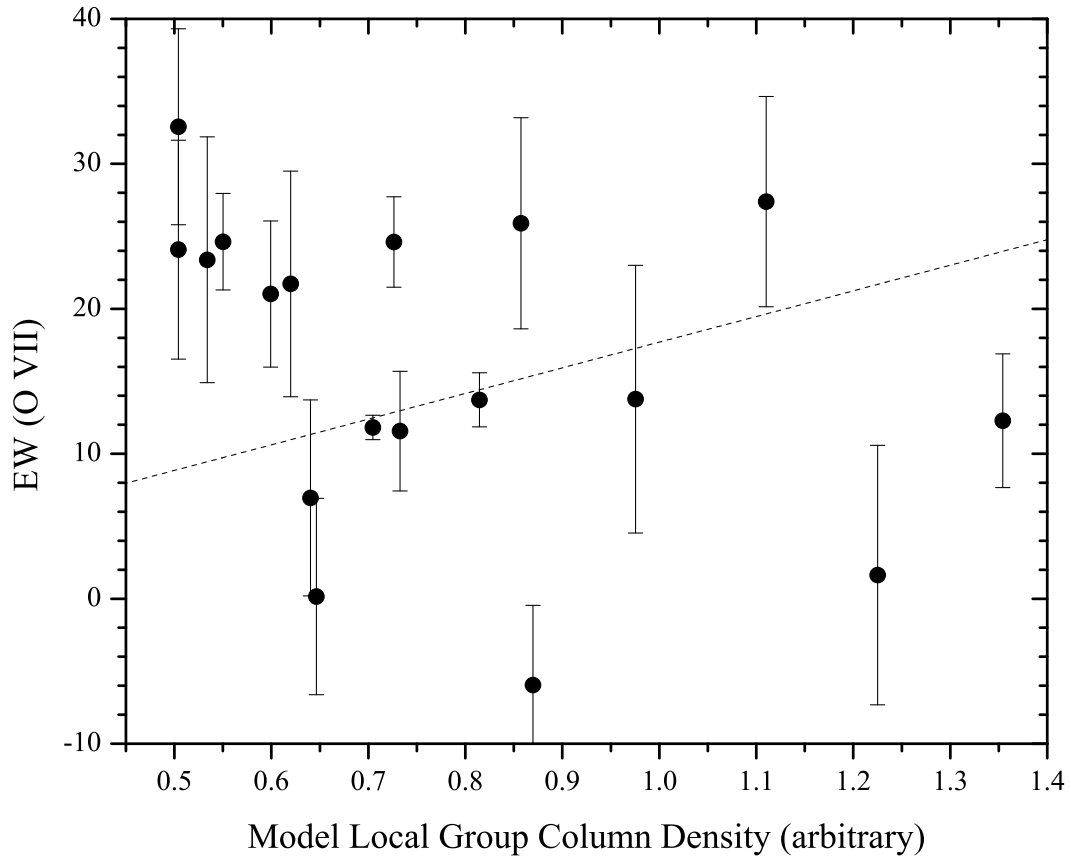


Fig. 8.— The observed O VII equivalent widths as a function of the column density of an ellipse of diffuse gas filling the Local Group and oriented along the Milky Way - M31 axis. The data are in conflict with the predicted distribution, shown as a dashed line.

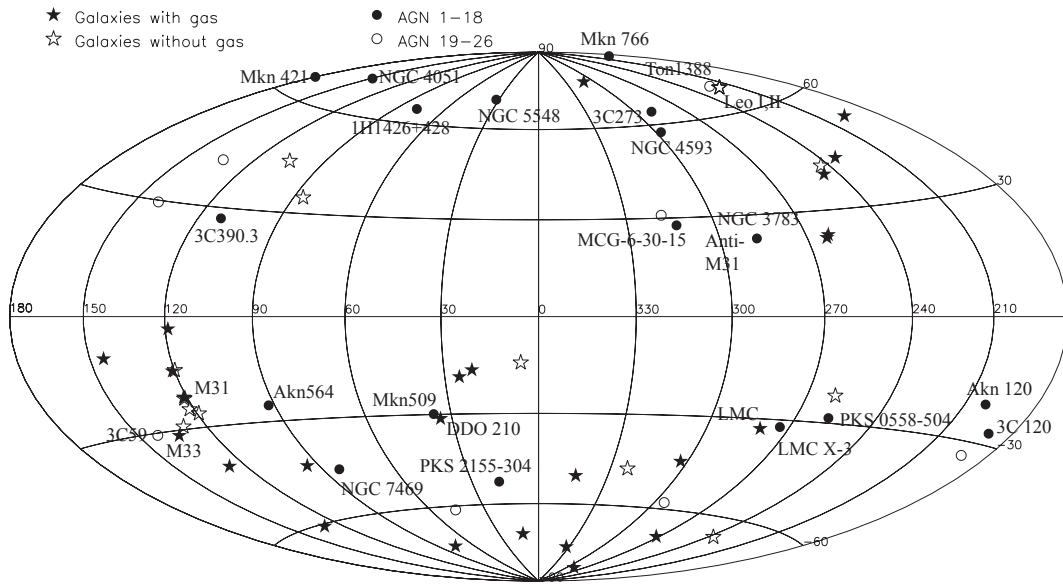


Fig. 9.— The distribution in the sky of the X-ray absorption sources (black circles are objects 1-18 and are labeled; open circles are objects 19-26) is shown along with the Local Group galaxies (stars; black indicates HI or H₂ gas was detected). Some of the prominent galaxies are labeled as are any moderately close galaxy-AGN pairs; the anti-M31 direction is labeled.

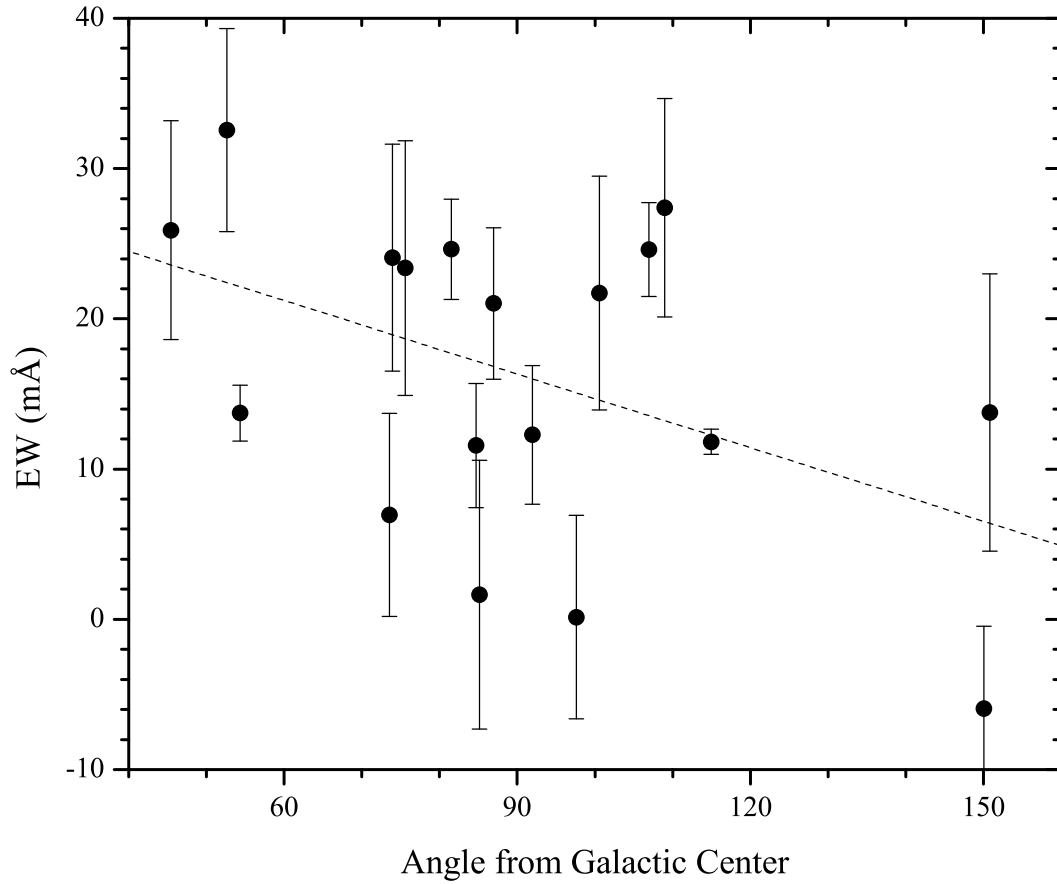


Fig. 10.— The O VII equivalent widths as a function of the angle from the Galactic Center, which shows a trend that is consistent with the Galactic Halo model. The dotted line is the best-fit, which is significant at the 95% level.

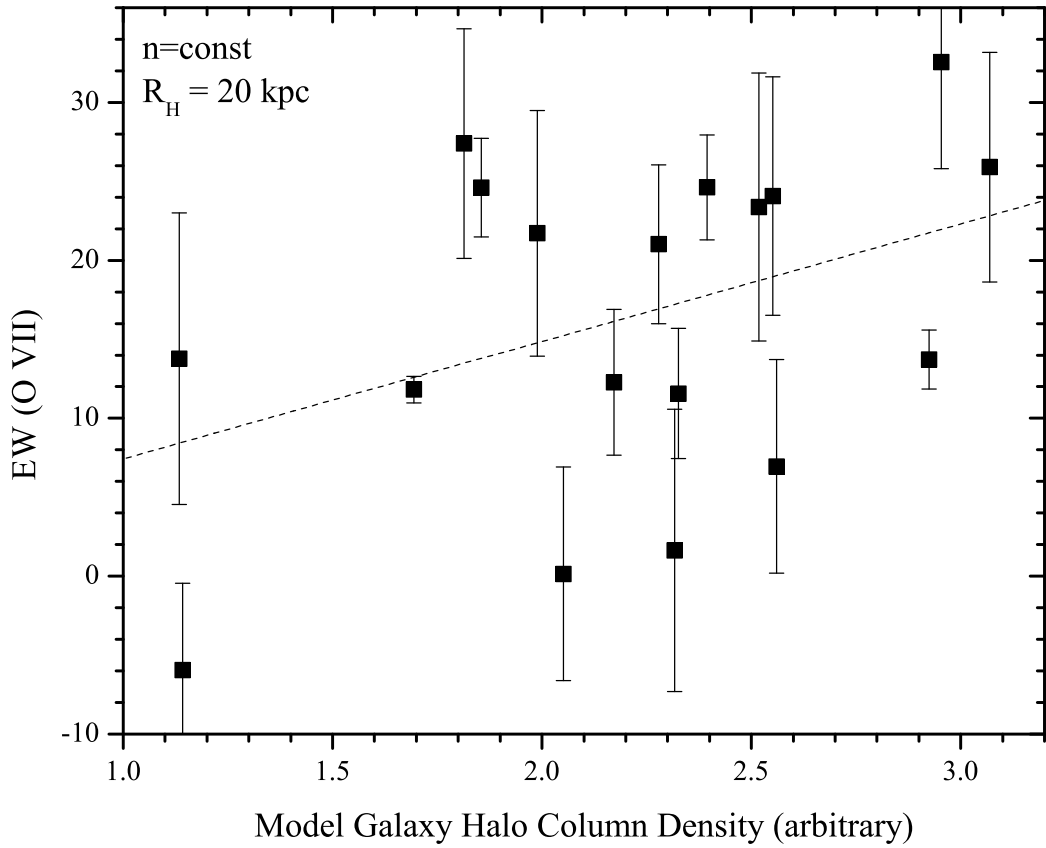


Fig. 11.— The O VII equivalent widths as a function of the column density for a Galactic halo of uniform density and radius of 20 kpc as measured from the Galactic Center. The model line passes through the origin and the fit is significant at the 95% level.

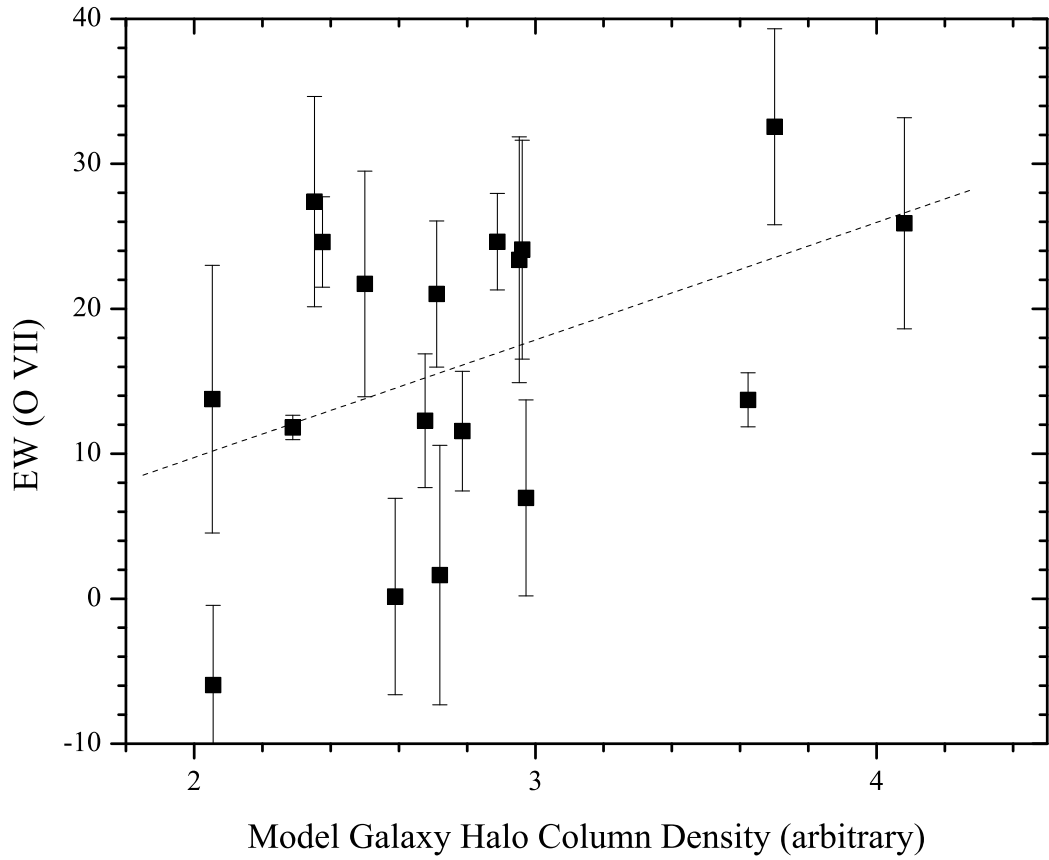


Fig. 12.— The O VII equivalent widths as a function of the column density for a Galactic halo where the density $n \propto r^{-3/2}$. The fit shown, which is not required to go through the origin is significant at the 95% level.

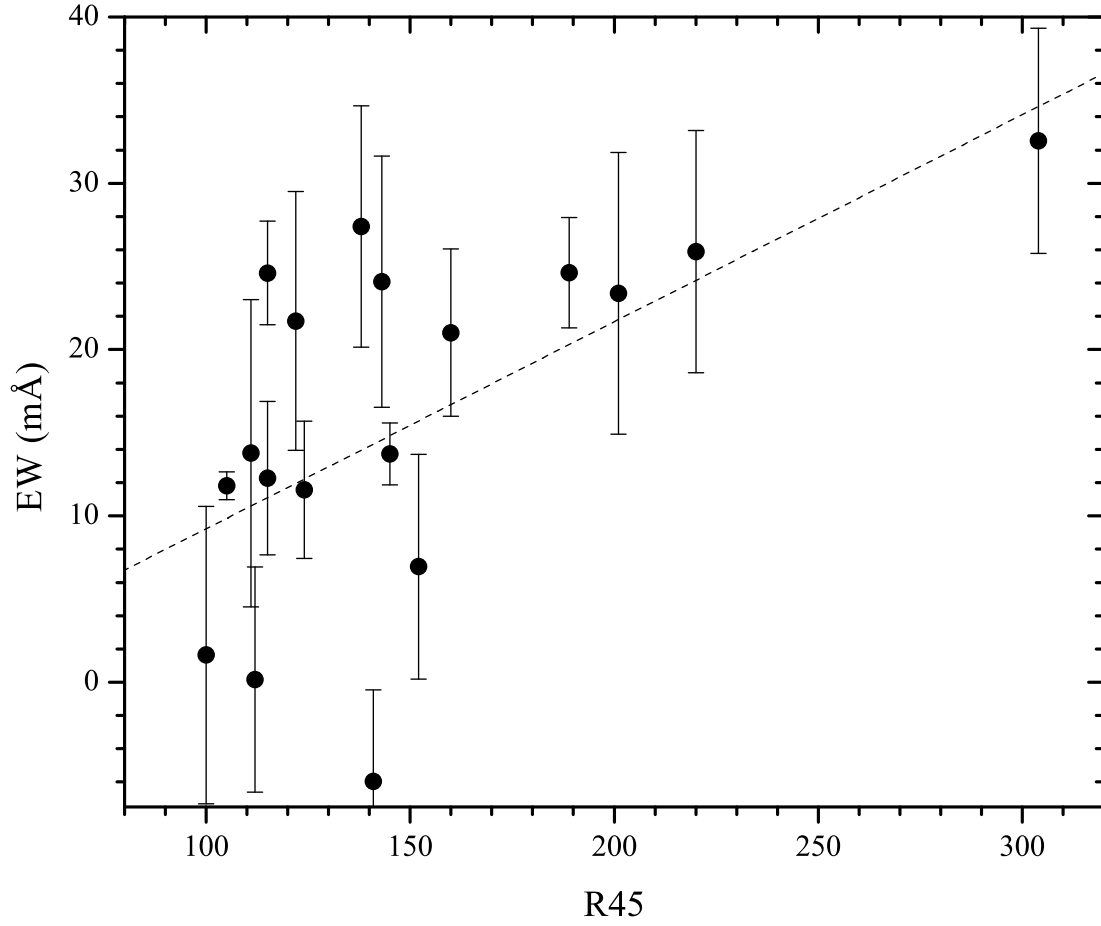


Fig. 13.— The O VII equivalent widths as a function of the R45 intensity in an annulus around each target; the units for R45 are 10^{-6} counts s^{-1} arcmin $^{-2}$. The fit (dashed line) is significant at the 98-99% confidence level.

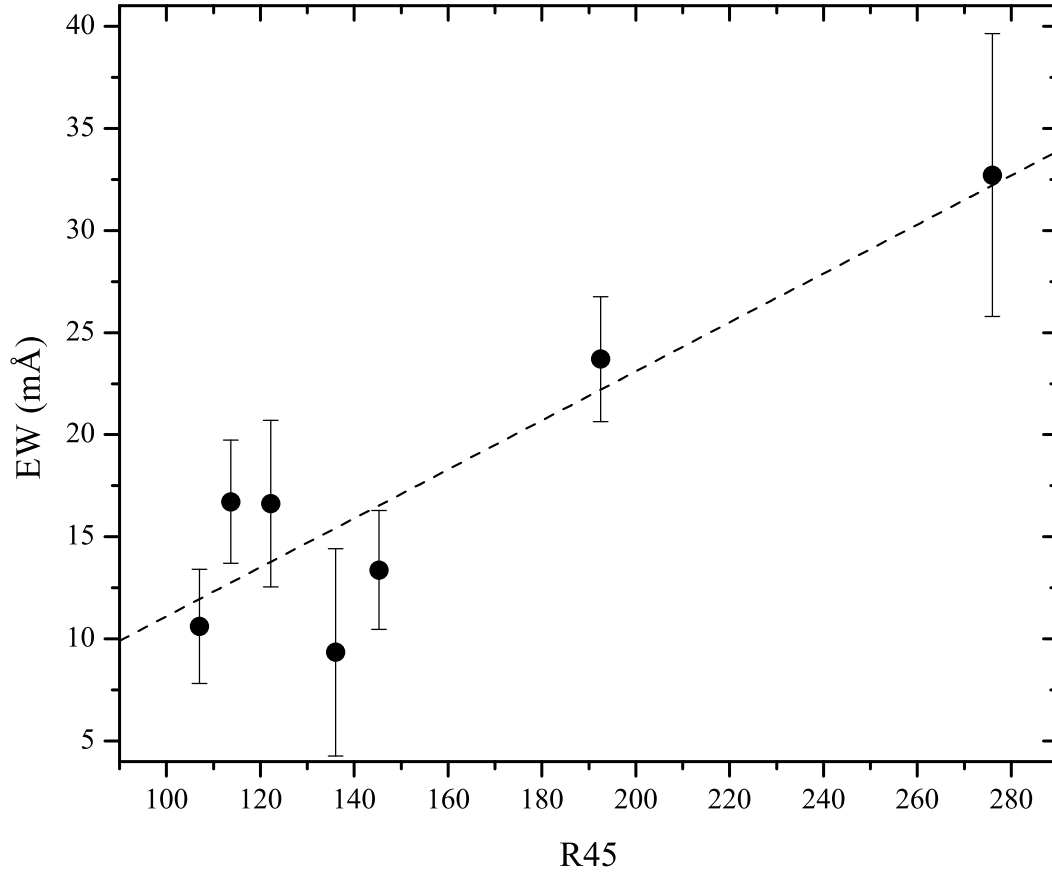


Fig. 14.— As above, except that all 26 objects are used to make binned, error-weighted averages. We have incorporated an additional rms to the equivalent widths of 3 mÅ so that the χ^2 of the error-weighted fit is in the acceptable range. The correlation is significant at the 99% confidence level.